Solvent effects on supercoiled DNA dynamics explored by Langevin dynamics simulations

Gomathi Ramachandran and Tamar Schlick*
The Howard Hughes Medical Institute and New York University, Chemistry Department and Courant Institute of Mathematical Sciences, 251 Mercer Street, New York, New York 10012
(Received 4 November 1994)

The dynamical effects of solvent on supercoiled DNA are explored through a simple, macroscopic energy model for DNA in the Langevin dynamics framework. Closed-circular DNA is modeled by B splines, and both elastic and electrostatic (screened Coulomb) potentials are included in the energy function. The Langevin formalism describes approximately the influence of the solvent on the motion of the solute. The collision frequency γ determines the magnitude of the friction and the variance of the random forces due to molecular collisions. Thus as a first approximation, the Langevin equation of motion can be parametrized to capture the approximate dynamics of DNA in a viscous medium. Solvent damping is well known to alter the dynamical behavior of DNA and affect various hydrodynamic properties. This work examines these effects systematically by varying the collision frequency (viscosity) with the goal of better understanding the dynamical behavior of supercoiled DNA. By varying γ over ten orders of magnitude, we identify three distinct physical regimes of DNA behavior: (i) low γ, dominated by globally harmonic motion; (ii) intermediate γ, characterized by maximal sampling and high mobility of the DNA; and (iii) high γ, dominated by random forces, where all of the global modes are effectively frozen by extreme overdamping. These regimes are explored extensively by Langevin dynamics simulations, offering insight into hydrodynamic effects on supercoiled DNA. At low γ, the DNA exhibits small, harmonic fluctuations. Transitions to other configurational regions are more difficult to capture in finite simulations. In the intermediate γ regime, the DNA exhibits maximal sampling of the writhe. Transition times are accelerated and more readily captured in the simulations. A preferential *lowering* of the writhe from the value at the potential energy minimum is noted, reflecting entropic effects. Only beyond a specific value of γ in this regime do we find reasonable convergence of the translational diffusion constants and velocity autocorrelation functions. This brackets the biologically relevant regime. At high γ the DNA supercoil fluctuates about two distinct regions of configuration space, one near the tightly wound potential energy minimum, the other related to more open configurations. Transitions between the two regions are infrequent. This behavior suggests two regions of free-energy minima (potential and entropically favored) separated by a barrier. Indeed, the general dependence of the extent of configurational sampling on the collision frequency is analogous to the isomerization behavior of a particle in a bistable potential modeled by the Langevin equation of motion. This intriguing parallelism suggests a favorable viscosity medium where specific internal modes, namely, global twisting, are activated. It is possible that physiological solvent densities correspond to this region of optimal mobility for the DNA.

PACS number(s): 87.15.–v

I. INTRODUCTION

An important facet of DNA's three-dimensional structure is supercoiling. In this supertwisted state, the DNA double-helical axis bends and twists about itself to form highly compact structures. Supercoiling relieves the induced torsional stress introduced by topology-regulating enzymes in closed-circular, or constrained, DNA systems. It thus condenses the DNA significantly and stores energy for readily performing important biological functions.

Experimental data on supercoiling comes from gel electrophoresis, electron microscopy, drug-DNA binding experiments, and other procedures [1–6]. However, the information obtained today is not of high resolution but rather indicative of overall trends, such as sensitivity to induced torsional stress and the ionic environment. Thus analytical models and computer simulations have continuously played a critical role in elucidating many interesting features of these intriguing DNA systems and connecting observations to biological processes (see recent reviews [7]).

Most of these analytical and numerical models rely on a macroscopic, elastic treatment of DNA. That is, the DNA is modeled as an elastic rod of circular cross section, with bending and torsional rigidity stiffness constants incorporated into harmonic potentials. Additionally, repulsive terms are usually added (e.g., van der Waals, Coulombic, hard sphere) to model excluded volume effects. Because

*Electronic address: schlick@nyu.edu

the DNA systems are large (thousands of base pairs), a statistical mechanical treatment is appropriate. That is, unlike small globular proteins that tend to fluctuate near well-defined native (folded) structures, supercoiled DNA systems are expected to be rather floppy, covering various supercoiled states that are thermally accessible in the natural environment. Interwound branching patterns, for example, are expected to change frequently and to depend on sequence composition as well as salt environment. Similarly, the damping effects introduced by the solvent are expected to alter DNA mobility and affect many hydrodynamic properties crucial to DNA function.

Our focus in this paper is on the *dynamics* of DNA supercoiling, particularly the influence of solvent viscosity on the global dynamical properties of DNA. Here we extend our previous macroscopic, B-spline model [8,9] to mimic crudely solvent effects in the Langevin formalism through the viscosity parameter. We emphasize that the potential energy is not changed in any way; only the coupling of the system to the heat bath is changed (see next section). Thus in principle, equilibrium properties will be unaltered, but dynamical properties will change. Moreover, in practice, as we shall see, appropriate viscosity modeling is computationally advantageous, since it can accelerate configurational sampling. Furthermore, the range of viscosity explored here provides insights into the dynamical behavior of DNA in vacuum versus those expected in solution.

The Langevin formalism, a modeling framework specifically developed to represent solvent interactions in a thermal reservoir [10,11], is used here to explore the dynamics of supercoiled DNA. In its simplest form, the Langevin equation consists of frictional and random forces in addition to the systematic forces. These terms mimic crudely thermal fluctuations and establish a target temperature. The key parameter γ, the collision frequency, controls the magnitude of the frictional term (proportional to the velocity) and the variance of the random force terms (details follow in the next section). This parameter can be selected from experimental measurements of viscosity and can be related to Stokes's law on the basis of hydrodynamic parameters (hydrodynamic radius and mass of a solute particle and the viscosity of the solvent).

In our previous works, a value for γ was chosen so as to focus on the intramolecular elastic and low-frequency modes of the DNA supercoil in order to understand first the "ideal" supercoiling response to torsional stress [8,9]. Since these harmonic motions are strongly damped by the solvent in reality, we now continue to investigate the effect of solvent damping on the low-frequency modes. Specifically, we rely on the analytical framework known for Langevin dynamics (spanning a range from inertial to diffusive regimes) and classical transition-rate theory to select an appropriate value of γ for our macroscopic model that qualitatively represents solvent overdamping. We then investigate systematically the influence of solvent viscosity on the dynamical behavior of DNA. Information is presented on the trajectory evolution as a function of γ, dynamical correlation functions, extent of configurational sampling, and translational diffusion constants. The behavior in a viscous medium is now far more interesting than that obtained at a low viscosity (*in vacuo*) environment: sampling is greatly enhanced, and the qualitative features of DNA floppiness in solvent and salt emerge readily in the dynamics simulations.

In the next section, we review the Langevin dynamics framework, crucial to our development of an appropriate solvent regime. The results and discussions are collected in Sec. III, and a brief summary is provided in Sec. IV. Further studies involving mode analysis by Fourier transforms and other biologically relevant properties are available separately [12].

II. LANGEVIN DYNAMICS

The Langevin dynamics formulation is described by the following pair of first-order differential equations:

$$M\dot{\mathbf{V}}(t) = -\mathbf{g}_E(\mathbf{X}(t)) - \gamma M\mathbf{V}(t) + \mathbf{R}(t), \tag{1a}$$

$$\dot{\mathbf{X}}(t) = \mathbf{V}(t), \tag{1b}$$

where M is the diagonal mass matrix; $\mathbf{X}$ and $\mathbf{V}$ are the collective coordinate and velocity vectors of the molecular system, respectively; $\mathbf{g}_E(\mathbf{X})$ is the gradient vector of the potential energy E; and $\mathbf{R}(t)$ is a random force vector, whose mean $\langle\mathbf{R}(t)\rangle$ is zero, and whose covariance matrix is given by

$$\langle\mathbf{R}(t)\mathbf{R}(t')^T\rangle = 2\gamma k_B T M\delta(t-t'). \tag{1c}$$

The damping constant γ (also called the collision frequency) controls both the magnitude of the frictional force and the variance of the random forces and therefore can mimic a thermal environment for the molecular system.

The Langevin equation of motion has had a long history in molecular modeling, originating from the study of liquids, polymers, and simple molecular reactions [11]. It provides a useful framework to study the dynamics of complex biomolecular systems today, such as proteins and lipid bilayer systems [10], since it attempts to describe in a simple and computationally feasible way the internal motions of a flexible molecular system in a solvent environment. Explicit modeling of water molecules and counterions requires very large amounts of computer time (since thousands of water molecules must be explicitly modeled) and, moreover, leads to many significant stability issues that must be resolved, especially in the context of highly charged nucleic acids [13,14].

In the simplest form of the Langevin dynamics equation, the friction kernel is assumed to be space and time independent for each particle, and hydrodynamic interactions are ignored. The influence of the environment on the systematic, internal force of the solute molecule is then represented in an average sense by incorporating effective frictional and restoring forces induced by

the solvent. These additional forces are dissipative and stochastic [see Eq. (1)], and the resulting equation can be integrated by the same techniques as used for molecular dynamics. However, a significant gain in computation time is possible in comparison to explicit-solvent formulations due to the reduction in the number of variables. Furthermore, the random force terms are well known to enhance configurational sampling [15].

For modeling supercoiled DNA, the macroscopic nature of our formulation makes the Langevin approach attractive. The effects of solvent, which tends to overdamp systematic motions of the DNA, must be included to obtain a physically realistic picture of DNA motion. As in standard Langevin simulations, the key parameter is the damping constant γ, but a straightforward parametrization is not available for our B-spline model as in all-atom simulation of proteins (where, for example, γ can be related to the accessible surface area of each atom and is in the range of 50 ps^{-1} [10]). However, a large body of work is available on the theory of the Langevin equation, and we will use it here to find the most appropriate value of γ for our system and then explore the associated dynamics.

The parameter γ affects the "strength" of the coupling between the solute and the thermal reservoir. When γ is small, the coupling is weak and, when γ is large, the coupling is strong. The nature of this coupling affects the behavior of the system and the rate by which equilibrium is reached. It does not, however, change the equilibrium itself, though in practice it can change the static averages obtained over a finite simulation time. At small γ, where the intramolecular potentials are dominant, inertial effects are important, and the system's trajectory follows closely the Newtonian trajectory ($\gamma = 0$). In this regime, the motion is typically underdamped ($\gamma < 2\omega$ for harmonic oscillators with natural angular frequency ω), and the energy lies close to the constant (conserved) value corresponding to the input temperature. In the limit of large γ, the motion is predominantly *diffusive*, or Brownian. The solvent environment overdamps the motion of the system, and inertial effects are small.

Figures 1 and 2 illustrate the influence of γ on the dynamics of a one-dimensional harmonic oscillator. In Fig. 1, we show the displacements in time (x vs t) obtained from Langevin trajectories at increasing values of γ; Fig. 2 displays the corresponding phase diagrams in position and momentum space. Clearly, the motions are harmonic (sinusoidal) at $\gamma = 0$, but as γ is increased, the solvent dephases the oscillator and leads to motion that becomes progressively more random [1(a)–1(d)]. At very high γ, solvent damping is so strong that the system becomes "frozen." These trends are clearly seen in the phase diagram series also. It should be emphasized that in Langevin, unlike molecular dynamics simulations, the energy is not conserved but fluctuates around the target value; the nature of these fluctuations (widths of envelopes, etc.) depends on γ. The greater the fluctuations, the easier it is in practice to capture a wider range of configurational states.

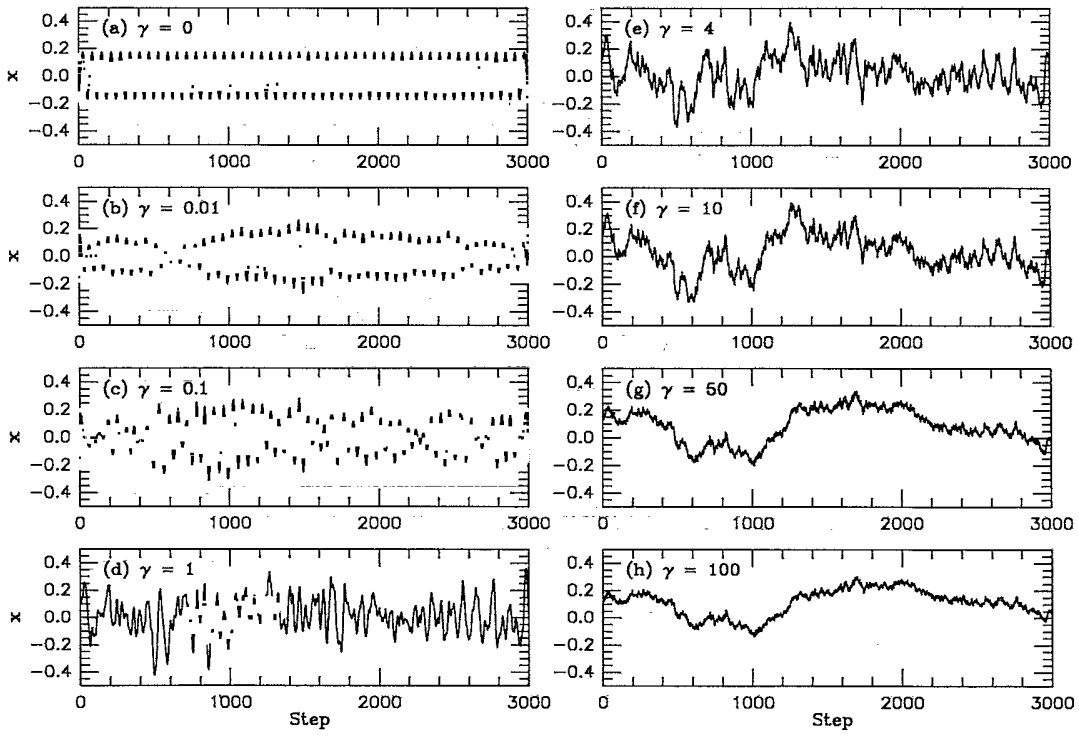

FIG. 1. Langevin trajectories for the harmonic oscillator: x vs t. The time evolution of the position (x) for the harmonic oscillator with potential energy $V = \frac{x^2}{2}$ (natural angular frequency $\omega = 1$ and unit mass), propagated by the Langevin dynamics equation [Eqs. 1(a), 1(b)], is shown for various γ between 0 and 100ω. The trajectories are propagated by the explicit (Verlet) scheme, with a time step of 0.1, roughly one 1/60 of a period.

The Langevin behavior can be analyzed in terms of the Fokker-Planck equation, a stochastic partial differential equation from which *probability distributions* of positions and velocities can be calculated [11,16]. In particular, in the high γ limit, the Fokker-Planck equation reduces to the diffusion equation. The Fokker-Planck equation can only be solved analytically for simple systems, such as harmonic oscillators, but provides a useful reference in many situations. In particular, the Fokker-Planck equation provides a valuable framework for studying the relationship between γ and simulated transition rates in simple systems [17]. The additional forces, such as in the Langevin model, are necessary to study efficiently transitions of a system in a solvent, such as the isomerization of butane [10], because the statistics of transition are better due to enhanced conformational sampling.

Transition-rate theory is also relevant to this work because the effect of γ (nature of the solvent coupling) on DNA motion can be analyzed similarly. Clearly, transitional motion for the DNA will be far more complex, involving different favorable (and related) configurational states and possibly also buckling phenomena [18]. According to transition-rate theory for the Langevin equation, at low γ inertial effects are too strong to be countered by the solvent and therefore transitions are infrequent and the rate low; as γ increases, the transition rate increases up to some critical value where the balance of intramolecular and solvent effects establishes a maximal transition rate; as γ increases beyond this point, the diffusive forces overwhelm inertial forces and the transition rate of the system decreases and plateaus to the diffusive limit.

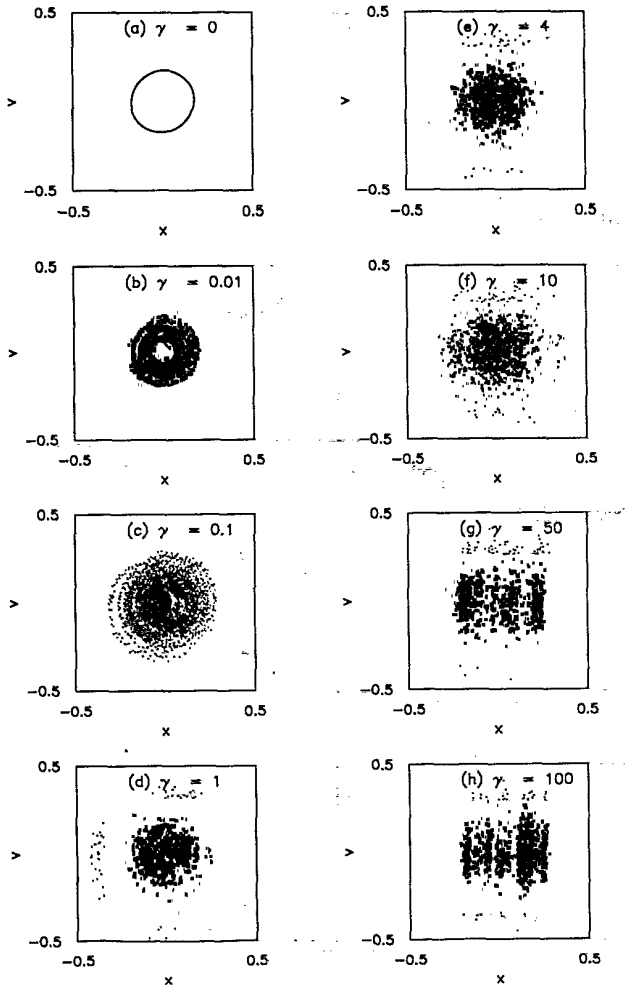

FIG. 2. Langevin trajectories for the harmonic oscillator: Phase space view. The momentum (v) is plotted as a function of the position (x) of the harmonic oscillator described in Fig. 1.

In Fig. 3 we show the dependence of the transition rate on the collision frequency γ for a one-dimensional bistable (double-well) potential. The curve is based on the analytical formulation of Mel'nikov and Meshkov describing the transition rate dependence on γ [19]. This result was obtained by reformulating the Fokker-Planck equation in terms of the action of the particle, S. The derived normalized transition rate is

$$\frac{k}{k_{TST}} = \sqrt{2}\left(\sqrt{\frac{\gamma^2}{2}+1}-\frac{\gamma}{\sqrt{2}}\right)\frac{A^2(\gamma S)}{A(2\gamma S)}, \qquad (2)$$

where $A(\beta)$ denotes an expression calculated by numerical integration [20]:

$$A(\beta) = \exp\left\{\frac{2}{\pi}\int_0^{\frac{\pi}{2}} \ln\left[1-\exp\left(\frac{-\beta}{4\cos^2 x}\right)\right] dx\right\}. \qquad (3)$$

The variable k_{TST} above is the transition-state theory value of the transition rate [21],

$$k_{TST} = \frac{\omega_b}{2\pi}\exp\left(\frac{-E}{k_B T}\right), \qquad (4)$$

where ω_b is the frequency of the barrier (equal to unity for the bistable potential studied [20]) and k_{TST} is the maximum value of the transition rate for a barrier height of E. Note from Fig. 3 that the same transition rate can be achieved at two different values of γ (lower and higher than the value corresponding to the maximal transition rate). At the optimum γ (highest transition rate), maximal sampling occurs. For this reason, appropriate values of γ, corresponding to maximal sampling, have been advocated for polypeptide Langevin simulations to obtain the most reliable statistics [15]. This will also be a goal in this work in addition to qualitative mimicking of solvent overdamping. Thus, if we could construct a picture analogous to Fig. 3 as a function of γ for our DNA system, an appropriate value of γ will fall slightly to the right of the value corresponding to maximal transition (sampling). The analysis below aims at this representation.

III. MODEL, RESULTS, AND DISCUSSION

Our DNA double-helical chain is represented by a B-spline curve [8]. The B-spline model can represent the DNA duplex curve in terms of a small number of con-

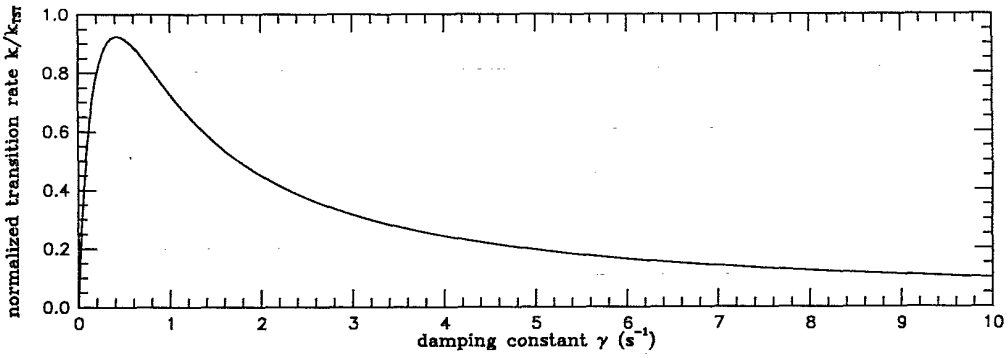

FIG. 3. The dependence of the transition-rate constant on γ for a bistable potential. The normalized transition rate (k/k_{TST}, where k_{TST} is the transition rate predicted by transition-state theory) is plotted as a function of γ for the particle in a bistable potential. See Eqs. (2)–(4) of the text for details.

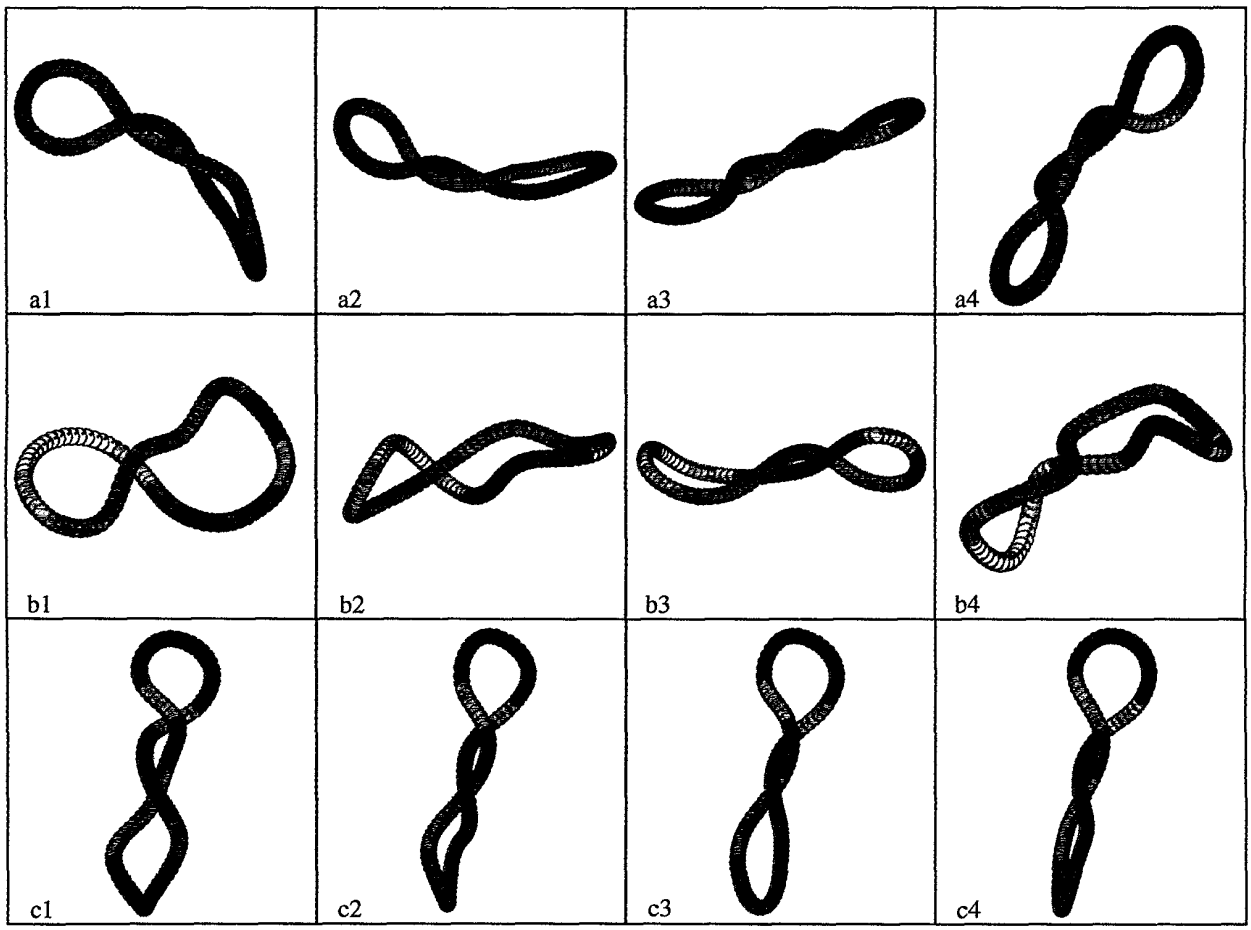

FIG. 4. Snapshots of supercoiled DNA dynamics. Four representative frames from each of three DNA trajectories with different values of γ are shown. The top, middle, and bottom rows (each in order of left to right) correspond to the three γ values of sets 1, 9, and 12 of Table I. The images were generated by the molecular graphics program MOLSCRIPT [22] in combination with the graphics interface written by Kreatsoulas.

trol points which are then used to define any given number of curve points [8] (see color Fig. 4 prepared with MOLSCRIPT [22]). The elastic-based energy function contains bending and twisting terms and a Debye-Hückel potential to represent screened Coulombic interactions [9]. Additionally, a harmonic term is included to ensure that the total chain length remains close to its target value. For further details of the representation and the potential energy function, see Refs. [8,9].

All simulations are reported for a 1000 base-pair DNA system, modeled by 14 B-spline control points, in a univalent salt concentration of $0.1M$ and a temperature of 300 K. The linking number difference ΔLk (a measure of torsional stress with respect to the relaxed state) was fixed at 5 for all simulations corresponding to typical magnitudes of physiological superhelical densities ($\sigma = \Delta\mathrm{Lk}/\mathrm{Lk}_0 \sim 0.05$) [8]. The elastic and electrostatic constants are used as in previous works: $A = 1.2755 \times 10^{-19}$ erg cm, corresponding to the nonelectrostatic contribution to the bending constant, along with $A/C = 1.5$ [9]. The varied parameter γ ranges from 10^3 s^{-1} to 10^{13} s^{-1}. Table I summarizes the various parameters used in the simulations. Each trajectory is started from the equilibrium interwound structure associated with a salt concentration of $0.1M$ and with $\Delta\mathrm{Lk} = 5$, as computed in Ref. [9] (see structures in Fig. 4, third row). This potential energy minimum was the lowest one identified by truncated Newton minimization from a variety of starting points. Another three-lobed minimum has been observed (with Wr = 1.97) with these parameters (higher in energy) [9], but we have not observed transitions to this family of structures during our simulations. Transitions between the interwound and the lobed structures must overcome a high energy barrier, one which will become easier to surmount for longer chain lengths. Indeed, this is supported by simulations for a 2000 base-pair DNA model [12]. In general, we expect more frequent transitions between various families of minima [18] for longer DNA chains. For a minimization and energetics study of the various DNA potential energy minima for our B-spline model, and related buckling catastrophes, see [18,9].

TABLE I. Trajectory parameters. All trajectories have a linking number difference $\Delta\mathrm{Lk} = 5$ and are started from the equilibrium structure (Wr = 2.05) in a salt concentration of $0.1M$. All simulations are performed using the LI integration scheme with an integration time step of τ (see text and Ref. [24]) for 60 000 iterations. The trajectories in set 12 were propagated twice as long (120 000 iterations) for Fig. 8.

Set	γ (s^{-1})	Number of Trajectories
1	9.77×10^{2}	1
2	9.77×10^{6}	1
3	9.77×10^{8}	4
4	3.52×10^{10}	1
5	4.79×10^{10}	1
6	6.25×10^{10}	1
7	9.77×10^{10}	4
8	1.52×10^{11}	1
9	3.91×10^{11}	4
10	8.80×10^{11}	4
11	2.44×10^{12}	1
12	9.77×10^{12}	4

We use the implicit ("LI") numerical scheme (Langevin–implicit-Euler) [23,24] to integrate the Langevin equation of motion. The input integration time step is $\tau = 2\Delta t$ ($\Delta t = 48.8888$ fs) but must be related to the physical time step by calibration [25]. Our best current estimate is $\tau \sim 1$ ns at moderate solvent damping [12]. LI provides a computational speedup of close to three in comparison to the explicit (Verlet) integration scheme. For example, on an SGI/Crimson computer with a 50 MHz IP17 processor, LI requires 5 h with a time step of τ to cover the same total simulation time as a Verlet integrator with a time step of 0.05τ for 120 000 iterations (14 CPU hours). Numerical damping issues [26] are only relevant here at very low γ values, because the high-frequency modes are generally absent, unlike all-atom systems.

A. Time evolution of the writhe

The writhing number (Wr) of the DNA supercoil is a geometric characteristic of shape that can be determined rigorously by the Gauss double integral [27]. Intuitively, this integral averages the number of signed self-crossings of the DNA duplex over an infinite number of projections [27]. To illustrate, a circle has a writhe of zero; an ideal figure-eight interwound structure has a writhe of one, and an ideal interwound supercoil with two superhelical nodes has Wr = 2. Of course, Wr is in general nonintegral. Since Wr is an important descriptor of DNA geometry and a conceptually meaningful parameter, we use the writhe of trajectories (evolution in time) and associated distributions to describe the nature and extent of conformational sampling during our molecular dynamics (MD) simulations.

In Fig. 5 we present the time evolution of the writhe, for a set of eight Langevin trajectories. The initial conditions for these trajectories are identical: each trajectory is started from the potential-energy-minimum (PEM) structure with Wr = 2.05; the trajectories differ only in the value of the collision frequency γ used in the Langevin equation (see Table I). Panels (a), (b), (c), etc., are labeled in the right-hand corner corresponding to the γ values in Table I, with 1 referring to the smallest value of γ (977.7 s^{-1}) and 12 referring to $\gamma = 9.77 \times 10^{12}$ s^{-1}.

Overall, the pattern of DNA fluctuations as a function of solvent damping (Fig. 5) resembles strikingly the pattern of Fig. 1 (bistable system). At small values of γ (resembling *in vacuo* environments) the fluctuations are nearly sinusoidal [panels (a) and (b)]; as γ is increased, a progressive dephasing occurs [panels (c)–(f)], and beyond a critical γ the system is essentially frozen [panels (g), (h)].

In the near-vacuum regime [panels (a)–(c)], the writhe fluctuates closely about the initial (PEM) writhe value. As mentioned above, numerical damping at low γ decreases the magnitude of the observed fluctuations. An explicit simulation performed at this γ regime reveals the same qualitative fluctuations in time but, over very long times, also samples regimes distinct from the potential

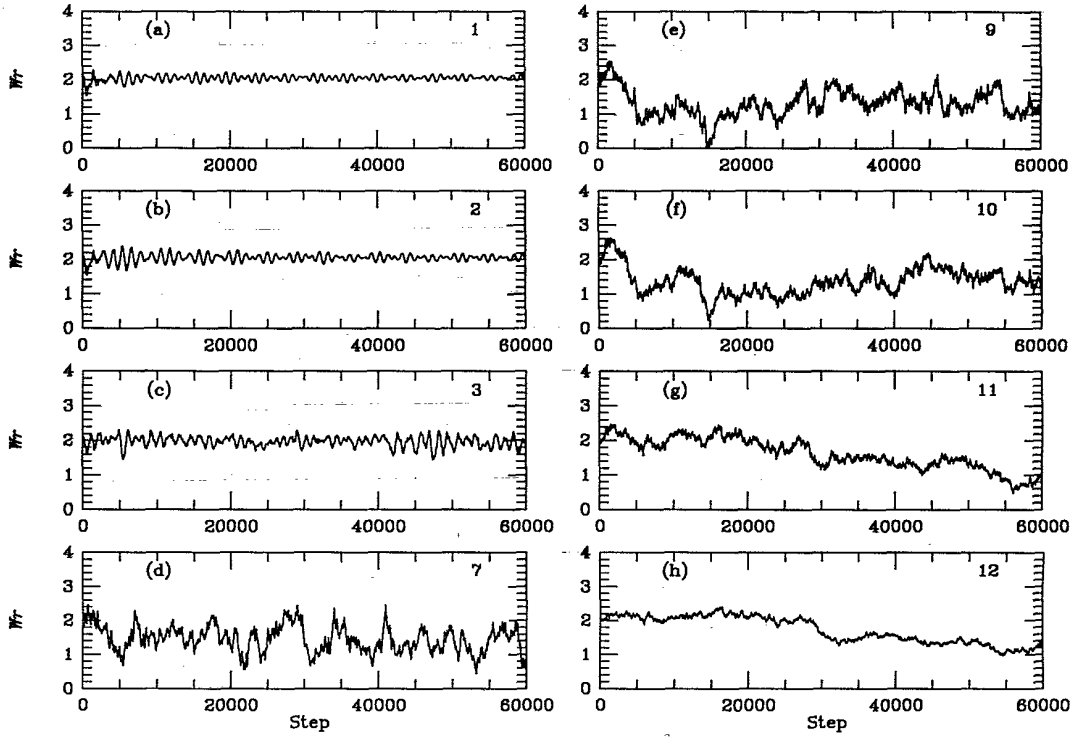

FIG. 5. Evolution of the writhe. The writhe (Wr) of the DNA as a function of time (iteration step) is shown for DNA trajectories started at the potential energy minimum (Wr = 2.05). Panels (a)–(h) show trajectories propagated with increasing values of γ. The number in the right-hand side of each panel refers to the corresponding γ for the trajectory (the "set" number) listed in Table I.

energy minimum. Note the striking sinusoidal "beat" pattern in panels (a) and (b), implying the existence of two close frequencies. As γ is increased beyond 9.77×10^{11} s^{-1}, the harmonic structure and the beat pattern of the time series are destroyed [panels (d)–(h)]. In panels (d)–(f) the writhe fluctuations are much larger than at other solvent densities. Close inspection of these fluctuations reveals another interesting trend: there is a preferential *lowering* of the writhe in these panels. Though writhe values above Wr = 2.05 can be noted, they are comparatively smaller and far more rare than deviations below Wr = 2.05. Furthermore, the trajectories in panels (d)–(f) tend to sample certain values of the writhe (1.0 <Wr< 1.5) more often than others. This selective lowering of the writhe is a consequence of entropic contributions and suggests the existence of a *free-energy* minimum at a lower writhe value. We will come back to this phenomenon later.

To reinforce these results, we examine the dynamics snapshots at the different solvent regimes (Fig. 4). The harmonic nature of the DNA motion at low γ clearly emerges from the views associated with $\gamma = 9.77 \times 10^2$ s^{-1} (set 1 of Table I), presented in the top row. Very elastic fluctuations—bending and twisting about the global helical axis—can be seen, as expected from an elastic material. The figures from the trajectory with higher γ (3.91×10^{11} s^{-1}, set 9 of Table I) shown in the middle row reveal very open, loosely supercoiled, and asymmetric forms. Thus the solvent-dependent lowering of the writhe is evident. In particular, the first two frames of the middle row show two frequently visited DNA configurations (Wr = 1.14, first frame, and Wr = 1.43, second).

These results demonstrate the profound influence of the solvent on the motion of DNA supercoils. In vacuum, or at low density of solvent, the DNA's motion is globally harmonic (bending and twisting about the long and short axes of the interwound structure, see [8]). As the density of the solvent increases progressively, such global modes are dephased steadily, until finally the motion of the DNA supercoil is completely dominated by the solvent collisions (e.g., see bottom row in Fig. 4). Moreover, the trend of writhe lowering due to thermal fluctuations clearly emerges.

B. Mean and standard deviation of the writhe

For each trajectory, we now calculate the average writhe and determine the associated error bars where possible. The accuracy of an equilibrium average $\langle A \rangle$ computed from a simulation of N steps can be estimated from the variance $\sigma^2(A)$, obtained from K trajectories that span the appropriate phase space:

$$\sigma^2(A) = \frac{1}{K}\sum_{k=1}^{K}(\langle A\rangle_k - \langle A\rangle_K)^2, \qquad (5)$$

where $\langle A\rangle_k$ is the average of A over trajectory k, and $\langle A\rangle_K$ is the average over all the K trials. Thus the length of the error bar is $|\sigma(A)|$. We compute this quantity for the five sets of four trajectories (associated with the same value of γ), as shown in Table I. Each trajectory in the set is started at the same (enthalpic-minimum) structure, but has different initial velocity assignments (same temperature, different random seed).

In Fig. 6 we plot on a logarithmic scale the mean writhe $\langle Wr\rangle$, and associated error bars, for the DNA trajectories (Table I). From this view, a very interesting pattern emerges. In the vacuous environment, the mean writhe coincides with the equilibrium value found by minimization ($Wr\simeq 2$). As solvent effects are incorporated, the mean Wr decreases due to entropic contributions. Indeed, we have demonstrated previously the thermal lowering of Wr during dynamics simulations [8,18]. However, this effect is very pronounced here. In particular, we see a notable minimum in $\langle Wr\rangle$ around 2×10^{10} $s^{-1} < \gamma < 2\times10^{12}$ s^{-1}. This result underscores the fact that dynamical means do not necessarily coincide with the static means when thermal fluctuations as well as external factors are incorporated [28]. The coupling to the heat bath affects substantially the rate at which equilibrium distributions are reached.

C. Barrier crossing

We plot in Fig. 7 the writhe envelope as a function of γ, showing both standard (top panel) and logarithmic (bottom) axes for γ. We define the writhe envelope as the mean deviation from the writhe of the PEM structure (as opposed to the deviation from the *average* writhe of the trajectory in the definition of the standard deviation σ). This notion of a writhe envelope can better estimate the extent of trajectory sampling than the standard deviation when, for example, the writhe distribution is bimodal or trimodal. We see a particularly broad peak for the Wr envelope in the region around 2×10^{10} $s^{-1} < \gamma < 2\times10^{12}$ s^{-1}, the same region where the lowering of the mean writhe is observed. The overall shape of this curve resembles closely the semianalytical pattern obtained for the transition rate in a bistable potential, shown in Fig. 3.

The shape of the writhe envelope as a function of γ and the evidence of a free-energy minimum, distinct from the zero-temperature enthalpic minimum, might suggest a condensed-phase reaction involving a barrier crossing, such as a particle governed by a bistable potential (Sec. II). Is it possible to analyze the pattern of conformational sampling observed here in terms of a barrier crossing event involving two minima, one narrow at the PEM form ($Wr = 2.05$) and one broader near $Wr\simeq 1.4$? Certainly, we expect the behavior of DNA to be much more complex than that of a particle in a bistable potential, but interesting analogies might be made.

To explore this intriguing connection, we show in Fig. 8 the time evolution of the writhe for five different trajectories in the high γ regime ($\gamma = 9.77\times10^{12}$ s^{-1}), all started at the PEM structure ($Wr = 2.05$) but differing in initial velocity assignments (different random seed). We observe a common pattern in these trajectories: the DNA remains near the starting configuration for around 20 000–30 000 iterations and then jumps to a new configuration ($Wr\simeq 1.4$) around which it oscillates for a long time (roughly 50 000 iterations) and then proceeds to a more open structure, the figure-eight interwound structure [panels (a), (b)] or to the tighter PEM form [panel (d)]. [In panel (c), fluctuations between $Wr = 1$ and 1.4 occur.] This pattern resembles strikingly a barrier crossing event. For reference, the total energy (bending, twisting, and Debye-Hückel) for the $Wr = 2.05$ form is 244.1 kcal/mol with associated components for bending and twisting of 5.55 and 6.19 kcal/mol, respectively. The states at $Wr = 1.4$ and 1.0 do not correspond to enthalpic minima at the superhelical density of the trajectory ($\sigma = 0.05$) and therefore have an associated *range* of energies. However, from an average of 4893 dynamically observed structures with $Wr = 1.40\pm0.03$, we obtain the estimate of 253.29 ± 1.98 for the total energy, 6.63 ± 0.82

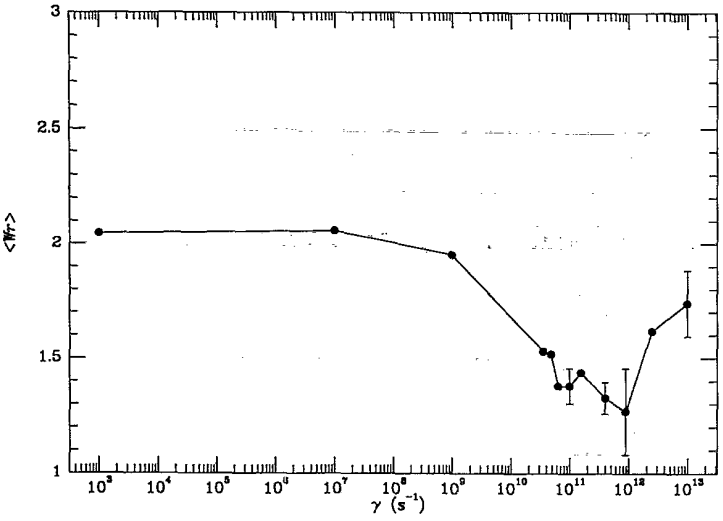

FIG. 6. The mean writhe $\langle Wr\rangle$ as a function of γ. Error bars are computed for the sets described in Table I where we have computed four trajectories. Thus there are error bars shown for sets 3, 7, 9, 10, and 12. The error bars for set 3 are so small that they are not visible; thus, we expect that error bars for $\gamma < 10^8$ s^{-1} (sets 1 and 2) would also be small [see Figs. 5(a) and 5(b), Eq. (5), and discussion in text].

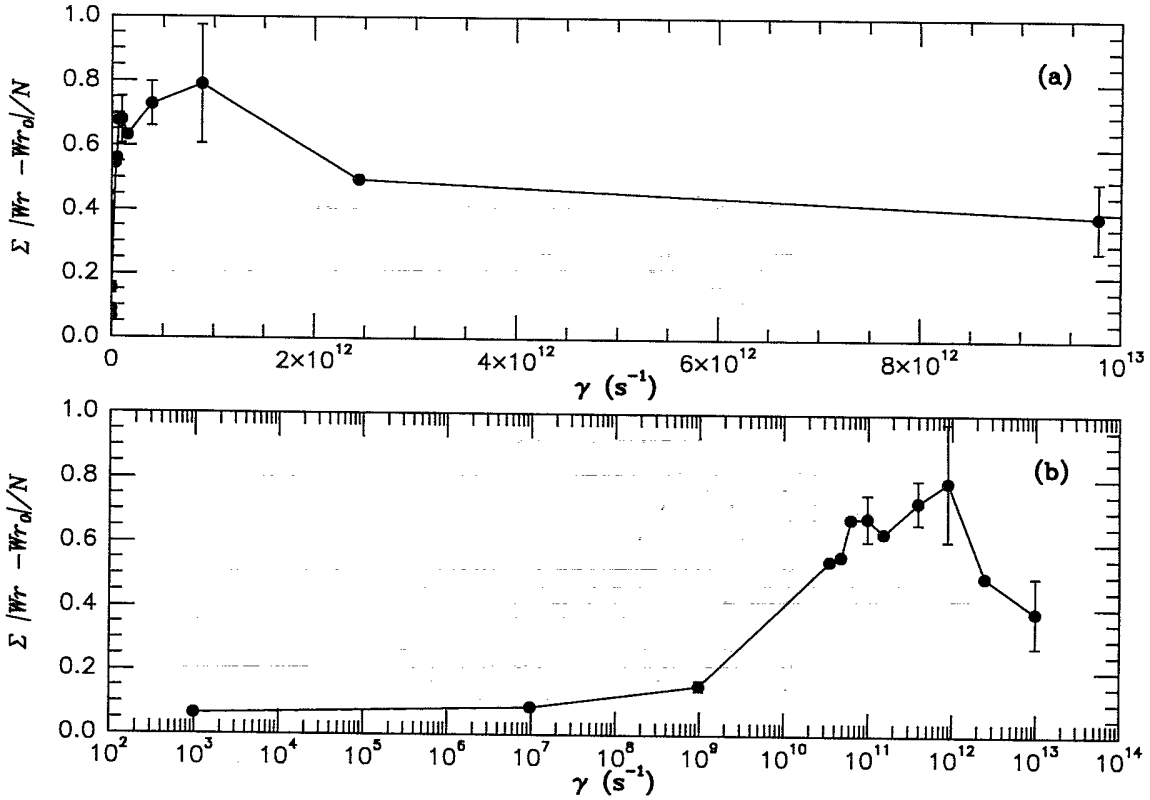

FIG. 7. Envelope of the writhe as a function of γ. The envelope of the writhe (measuring deviation from the starting structure) as a function of γ is plotted on (a) a standard axis for γ, and (b) a logarithmic axis. Error bars are plotted, as in Fig. 6 (see caption), for trajectory sets 3, 7, 9, 10, and 12. Note the similarity between the standard view [panel (a)] and Fig. 3.

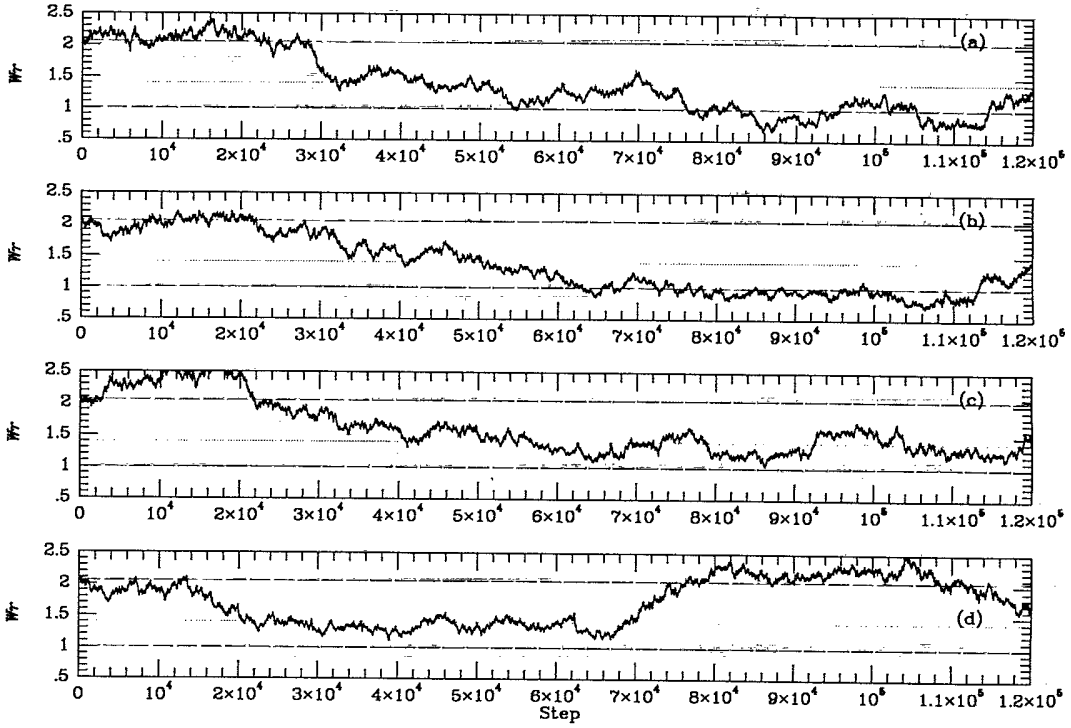

FIG. 8. Evolution of the writhe for trajectories in the high γ regime. The writhe is plotted as a function of the iteration number for four trajectories with $\gamma = 9.77 \times 10^{12}\ s^{-1}$ (set 12 of Table I). All trajectories move from the starting, potential energy minimum to a lower writhe configuration, which is entropically favored, after about 20 000 to 30 000 iterations. Some trajectories also visit the more open figure-eight interwound structure (Wr$\simeq$ 1).

for the bending energy (E_B), and 9.20 ± 0.15 for the twist energy (E_T). Similarly, for an average over 3753 structures with Wr = 1.00 ± 0.03, we obtain the estimate of 254.0 ± 1.92 for the total energy, 5.72 ± 0.82 for E_B, and 11.36 ± 0.16 for E_T (all units in kcal/mol).

For the particle in a bistable potential, the maximum sampling is found for $\omega/\gamma \simeq 2.9$ [20,10], where the angular frequency $\omega = 2\pi\nu$ with ν denoting the frequency of the barrier. Using this estimate and our observation that the broad maximum in the writhe envelope occurs at $2 \times 10^{10}\ \mathrm{s}^{-1} < \gamma < 2 \times 10^{12}\ \mathrm{s}^{-1}$, we estimate the frequency of the DNA reaction mode to be in the range $9 \times 10^{9}\ \mathrm{s}^{-1} < \nu < 9 \times 10^{11}\ \mathrm{s}^{-1}$. This is a broad range of solvent density, but we expect the relevant frequency, $\nu \simeq 2.9\gamma/2\pi$, to be at the lower end of this range. On the basis of visual inspection of the trajectories, we speculate that the excitation of a global twisting mode leads to the conformational sampling seen in the writhe fluctuations. This slow mode has a frequency of roughly $9 \times 10^{9}\ \mathrm{s}^{-1}$.

Another observation that might point to a free-energy barrier between the two preferred forms noted above is the configuration profile obtained as a function of ΔLk [9]. At the salt concentration examined here, two configurational regimes were identified: the figure-eight family (with Wr ranging from 0.9 to 1.2) and the interwound family with two self-crossings (Wr between 1.6 and 2.2) ([9], Fig. 5). Thus the unfavorable range of Wr values between 1.2 and 1.6 was associated with a "buckling" catastrophe, an abrupt change from a point to a line of contact [18]. This transition occurs with a sudden rise of bending energy accompanied by a sharp drop in twist energy. Although the superhelical density is fixed in our dynamical simulations, and thermal fluctuations make possible a wider range of stable forms, this interplay between the bending and twisting energy may contribute here also to an energy barrier.

D. Writhe autocorrelation

To examine the detailed dynamical fluctuations at each solvent environment, we examine the writhe autocorrelation functions for the DNA simulations. The unnormalized autocorrelation function for Wr is given by

$$C_{\mathrm{WrWr}}(t) = \langle \mathrm{Wr}(0)\mathrm{Wr}(t) \rangle - \langle \mathrm{Wr} \rangle^2, \tag{6}$$

where $\langle \mathrm{Wr} \rangle$ denotes the mean writhe over the trajectory. For highly correlated data, it is better to subtract the mean from the trajectory values before ensemble averaging [29] to result in

$$C_{\mathrm{WrWr}}(t) = \langle\, [\mathrm{Wr}(0) - \langle \mathrm{Wr} \rangle]\, [\mathrm{Wr}(t) - \langle \mathrm{Wr} \rangle]\, \rangle. \tag{7a}$$

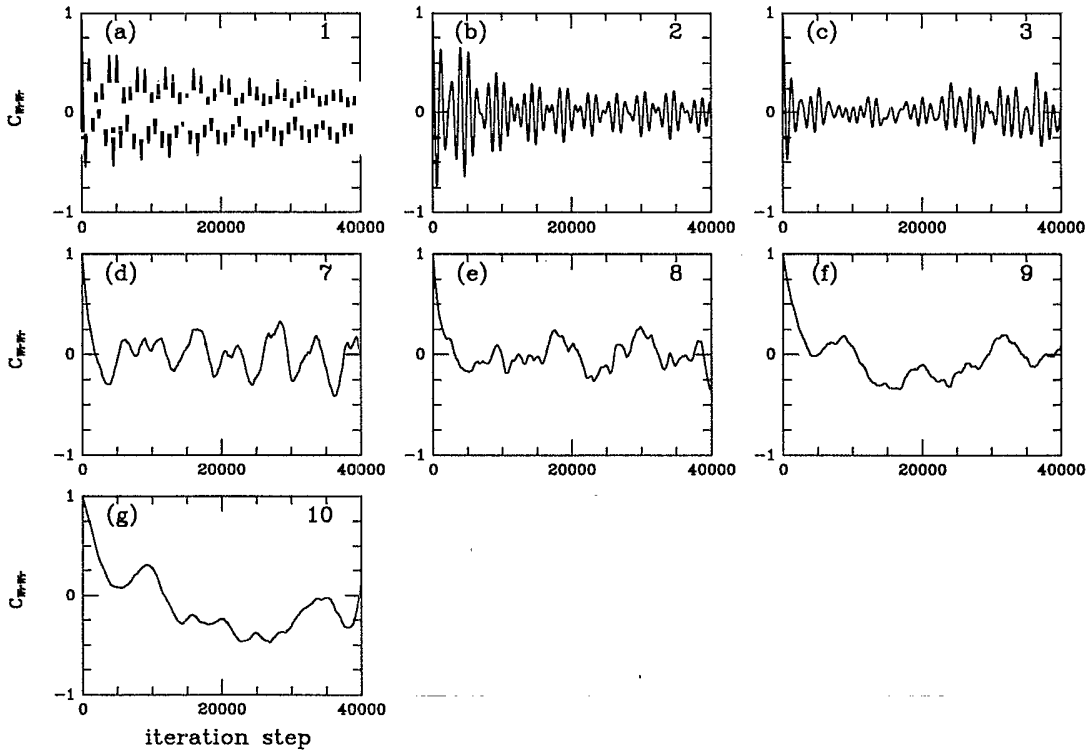

FIG. 9. Writhe autocorrelation functions as a function of γ. The writhe autocorrelation function [see Eqs. 7(a), 7(b)] is plotted as a function of iteration for seven trajectories of different γ. The number in the right-hand corner of each panel refers to the γ set listed in Table I. Writhe autocorrelation functions for trajectories with $\gamma > 8.8 \times 10^{11}\ \mathrm{s}^{-1}$ could not be computed accurately as the DNA is so immobile at this solvent density (see Fig. 4, bottom row) that there are few statistical samples per trajectory.

Thus the normalized autocorrelation function is given by

$$\overline{C}_{\mathrm{Wr}\mathrm{Wr}}(t) = C_{\mathrm{Wr}\mathrm{Wr}}(t)/C_{\mathrm{Wr}\mathrm{Wr}}(0). \quad (7b)$$

We present, in Fig. 9, the writhe autocorrelation functions [Eqs. (7a) and (7b)] for nine selected trajectories (labeled according to the corresponding γ value listed in Table I). The effects of viscosity on the configurational sampling of DNA are dramatic. In vacuum [panel (a)], the correlation function is highly harmonic, much like a set of *correlated* harmonic oscillators. The sinusoidal behavior can still be seen at low solvent densities [panels (b), (c)], but damping and collision-driven dynamics increase as more solvent-solvent and solvent-solute collisions are considered. Furthermore, different qualitative patterns emerge at low medium and high-density solvent environments. At the intermediate γ values examined here [$\gamma = 9.77\times10^{10}$, 1.52×10^{11}, and 3.91×10^{11} s^{-1}; panels (d), (e), (f), respectively], the rapid oscillatory behavior of $\overline{C}_{\mathrm{Wr}\mathrm{Wr}}(t)$ at the vacuous range is replaced by a slowly oscillating and decaying function. Thus correlations still remain over the entire simulation (60 000 iterations) at this solvent regime, but are not as pronounced as in the harmonic-elastic regime [panels (a)–(c)]. As viscosity increases, the dynamical quantities decorrelate steadily and slowly [panel (g)] until, at high viscosity, the DNA becomes so immobile (see bottom row of Fig. 4) that it is not possible to compute a reasonable writhe autocorrelation function for this length of simulation (essentially all points are correlated). Here, DNA motions are so strongly dominated by random forces that inertial forces play an insignificant role in directing mobility. Any concerted motion needed to twist or untwist the interwound structure (to reach other conformational states) cannot be sustained.

To further quantify the behavior of the writhe autocorrelation function, we estimate the standard deviation of Wr, over a single trajectory, by the procedure described below. Further analysis is warranted because the fluctuations in writhe reflect a concerted motion of the DNA, one of the slowest modes of the system. Indeed, in general, our trajectories are not much longer than the decorrelation time of the writhe, τ_{Wr} (estimated by the procedure described below).

Ideally, the standard deviation computed by Eq. (5) serves as an indicator of the accuracy of an equilibrium average computed from a set of simulations. In practice, however, the statistics obtained from large-scale biomolecular simulations are limited by computer time. Even if the computational limitations were overcome, the issue of correct (microcanonical or canonical) sampling of the phase space, for even small systems, is challenging and forms an active area of research [30]. Thus it is useful to estimate $\sigma^2(A)$ from one simulation [10]. The time correlation functions described above provide the basis for such an estimate. For a single trajectory of length T_{run}, the estimated variance for a property A, $\hat{\sigma}(A)$, can be obtained from [10]

$$\hat{\sigma}^2(A) = \frac{2}{T_{run}} \int_0^{T_{run}} \left[1 - \frac{t}{T_{run}}\right] \overline{C}_{AA}(t)dt, \quad (8)$$

where $\overline{C}_{AA}(t)$ is the corresponding correlation function. In the event that the trajectory is much longer than the decorrelation time τ_A, defined as [10]

$$\tau_A = \int_0^{\infty} \frac{\langle A(0)A(t)\rangle - \langle A\rangle^2}{\langle A^2\rangle - \langle A\rangle^2}\, dt, \quad (9)$$

it can be shown that Eq. (8) for the variance in terms of the autocorrelation function reduces to a simpler expression in terms of $\langle A\rangle$ and $\langle A^2\rangle$:

$$\hat{\sigma}^2(A) \simeq \frac{2\tau_A}{T_{run}}[\langle A^2\rangle - \langle A\rangle^2]. \quad (10)$$

This formula can be interpreted as the "error in the mean" for a set of $T_{run}/2\tau_A$ independent samples.

From the autocorrelation functions shown in Fig. 9, we calculate $\hat{\sigma}(\mathrm{Wr})$ for each trajectory [Eq. (8)] and from this, estimate τ_{Wr} using Eq. (10). We plot these two quantities in Fig. 10, with the right-hand ordinate showing the units for $\hat{\sigma}(\mathrm{Wr})$, and the left-hand ordinate showing those for the estimated decorrelation time $\hat{\tau}_{\mathrm{Wr}}$. This figure provides a more quantitative measure of the degree of conformational sampling expected at different solvent

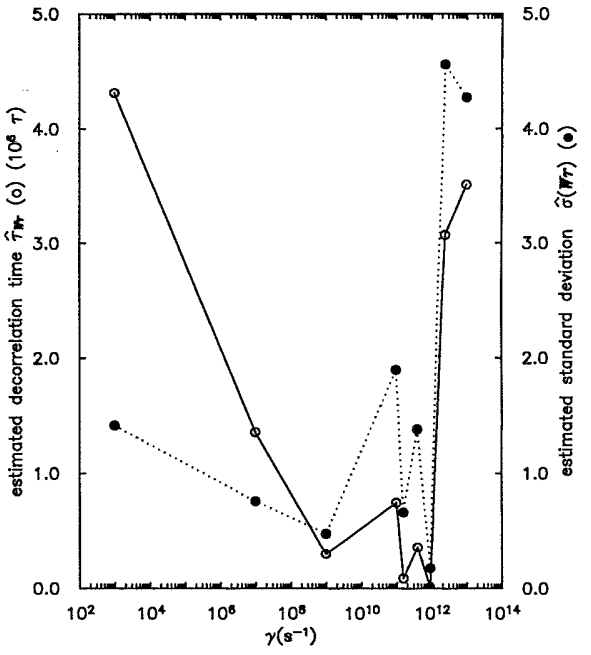

FIG. 10. Estimated writhe decorrelation times and estimated standard deviation as a function of γ. The writhe estimated decorrelation times $\hat{\tau}_{\mathrm{Wr}}$ are computed from the estimated standard deviation [$\hat{\sigma}(\mathrm{Wr})$] over one trajectory [Eq. (8)] and the relation of the estimated standard deviation to the mean and variance of the writhe over a single trajectory [Eq. (10)]. The writhe decorrelation times are reported in units of iteration on the left-hand ordinate (o). The estimated standard deviation [computed from the autocorrelation functions using Eq. (8)] is plotted on the same plot (•) with the right-hand ordinate showing the scale in units of the writhe.

environments: the lower the value of $\hat{\tau}_{\mathrm{Wr}}$ the greater the sampling. Thus maximal sampling appears in the medium γ range, as identified by Fig. 9. Note how the estimated error in the mean $[\hat{\sigma}(\mathrm{Wr})]$ can be small when the estimated decorrelation time $(\hat{\tau}_{\mathrm{Wr}})$ is large; this will be the case when the fluctuations around the mean value are small, even though fluctuations are highly *correlated*, as in the harmonic (small γ) regime. Similarly a small relaxation time $\hat{\tau}_{\mathrm{Wr}}$ can be associated with a large *estimated* error in the mean, due to the large fluctuations (intermediate γ regime). This large estimated error does not necessarily imply poor statistics: as we see in Fig. 6 the error in the mean $[\sigma(\mathrm{Wr})]$ computed in the standard fashion [Eq. (5)] is fairly small in the intermediate γ regime. A high $\hat{\sigma}(\mathrm{Wr})$ in this case indicates that a mean reflects several configurational states.

The autocorrelation functions together with the error approximations and estimated decorrelation times of the writhe demonstrate strikingly the influence of γ on the *dynamical* behavior of our DNA. At low *and* high γ regimes, trajectories are essentially correlated (in Wr) for all times; it is only in the intermediate γ regime that decorrelation occurs to any significant extent. Figures 9 and 10 show clearly that DNA fluctuations in the intermediate solvent regime reflect the widest conformational sampling. Thus equilibrium distributions are more readily attained in finite simulation times.

E. Velocity autocorrelation functions

The role of viscosity in maintaining or destroying various dynamical properties can be further examined through the autocorrelation function of the trajectories' velocities. We calculate the normalized velocity autocorrelation function, defined as

$$C_{VV}(t) = \langle \mathbf{V}(0) \cdot \mathbf{V}(t) \rangle - \langle \mathbf{V} \rangle^2 / [\langle \mathbf{V}(0) \cdot \mathbf{V}(0) \rangle - \langle \mathbf{V} \rangle^2], \tag{11}$$

where $\mathbf{V}$ is the velocity vector, $\langle \mathbf{V} \rangle$ denotes the mean velocity over time, and the dots indicate vector inner products. Two methods of averaging are possible: based only on the center of mass velocities ($\mathbf{V}_{c.m.}$), or involving all velocity vectors of the independent variables (curve points in our representation). Averaging over each curve point has the advantage of revealing the time-dependent pattern among the DNA curve points.

In Fig. 11 we first present the velocity autocorrelation functions computed using the center of gravity vectors for nine trajectories (Table I). In panels (a)–(c) of Fig. 11, correlations throughout the entire trajectory are indicated. This is expected in the harmonic, elastic regime. In panels (d)–(f) decorrelation is much faster (note the scale on the abscissa is ten times shorter to resolve the decorrelation), though some small correlations do persist

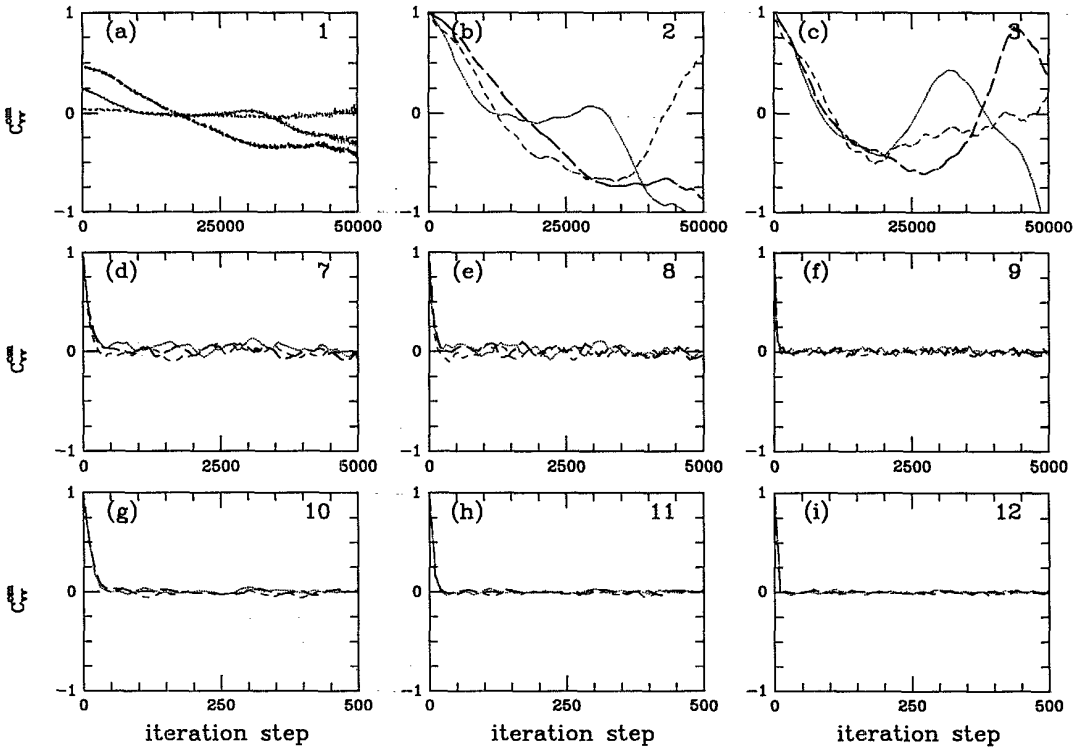

FIG. 11. Velocity autocorrelation functions averaged over center-of-mass (c.m.) vectors of the DNA chain. Velocity autocorrelation functions are computed using the center-of-mass vectors in Eq. (11) and plotted as a function of the iteration, for trajectories of different γ. The x, y, and z components of the autocorrelation function are plotted separately; the thick dashed line (— — —) represents the x component; the dotted line (···) the y component; and the short-dashed line (- - -) the z component. The numbers in the right-hand corner of each panel refer to the set number in Table I. Note the change of scale in the abscissa in each row of panels.

for a short time. Thus solvent acts to quickly damp out dynamic correlations in the system. At high viscosity [Figs. 11(g)–11(i)] velocity decorrelation occurs almost instantaneously (again note the change of scale of the abscissa).

Next, Fig. 12 shows the velocity autocorrelation functions computed by averaging over the curve points. The origin of the long time correlation in the harmonic regime [Figs. 11(a)–11(c)] is clearly due to the extensive correlations between *curve points* [see Figs. 12(a)–12(c)]. This is expected in a closed elastic material, where a stretch in one region commands a response in another. At medium and high solvent density environments, positional correlations along the chain are much weaker [compare Figs. 12(d)–12(i) to 11(d)–11(i)].

F. Translational diffusion constants

One available hydrodynamic measurement for DNA is the translational diffusion coefficient D_t [5]. This quantity, a measure of overall mobility, can be estimated by using dynamic light scattering for linear and supercoiled DNA molecules as a function of length and salt concentration. There are several ways to calculate D_t from computer simulations: from velocity autocorrelation functions, Fourier transforms [31], or root-mean-squared fluctuations [32]. Here we estimate D_t over long trajectories of length t, by the Einstein-Stokes expression:

$$6tD_t(t) = \langle \mid \mathbf{X}_{c.m.}(t') - \mathbf{X}_{c.m.}(t'+t) \mid^2 \rangle, \qquad (12)$$

where $\mathbf{X}_{c.m.}$ is the center of mass position vector of the DNA supercoil.

In Fig. 13 we plot the translational diffusion constants $D_t(t)$ for nine trajectories (Table I). The value of D_t shown at each time t reflects an average over all possible subtrajectories of length t [i.e., over many starting points t' in Eq. (12)]. The three patterned lines in Fig. 13 correspond to diffusion constants along the x, y, and z axes, and the thick solid line corresponds to the averaged quantity over the three directions. The function D_t is reported in units of m^2/τ, where τ is our integration time step. Again, we clearly identify three distinct regimes for supercoiled DNA: (1) the low viscosity regime [panels (b) and (c)] where D_t has not converged by the end of the trajectory, (2) the intermediate viscosity regime where D_t converges in the time span of the simulation, and (3) the high viscosity regime where D_t converges rapidly due to the dominance of random forces. Note that the trajectory with $\gamma = 9.77 \times 10^2\ s^{-1}$ [panel (a)] appears to have a small, converged value for D_t; this results from uncompensated numerical damping, which occurs at very low values of γ [23].

In many of the views, a dominant direction emerges corresponding to the x axis of the DNA supercoil, which exhibits maxima and possibly minima (at medium solvent density). This can be explained by the initial positioning of the long extended interwound along the x axis.

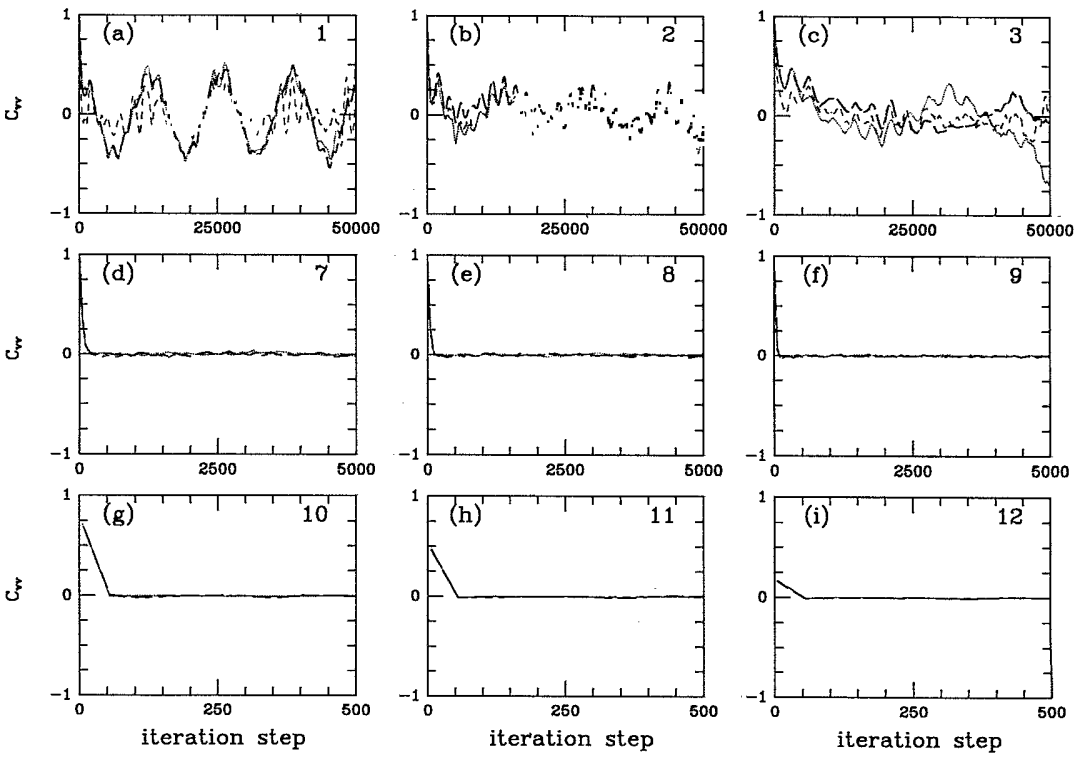

FIG. 12. Velocity autocorrelation functions averaged over all curve points of the DNA chain. Velocity autocorrelation functions are computed using the curve point vectors in Eq. (11) and plotted as a function of the iteration. The x, y, and z components are labeled as in Fig. 11 (see Fig. 11 caption).

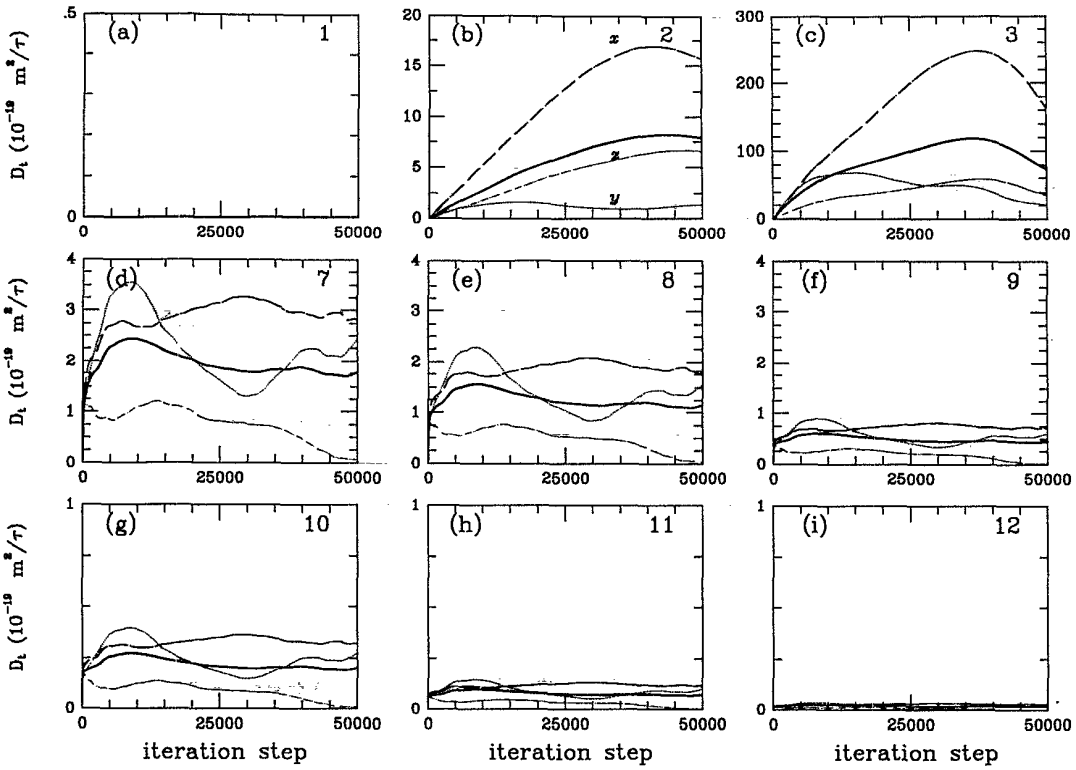

FIG. 13. Translational diffusion coefficients for the various γ regimes. Translational diffusion coefficients (D_t) are computed using Eq. (12) and plotted as a function of the iteration. The x, y, and z components of the velocity autocorrelation function are plotted separately and are marked in panel (b) [in panel (a) the lines are indistinguishable].

In the harmonic regime [panels (b), (c)], D_t tends to a large value, but convergence has not been achieved during the course of the simulation. The long time correlations, evident in the velocity autocorrelation functions for this regime [Figs. 11(b) and 11(c) and 12(b) and (c)], indicate that an estimation of D_t from trajectories of such length is impossible [31]; a much longer trajectory or possibly an ensemble of trajectories is necessary to compute D_t in the low γ regime.

At higher viscosity environments ($\gamma > 9.77 \times 10^8$ s^{-1}) the translational diffusion constant behaves as expected: monotonic decrease with increasing γ, due to increase of random forces. In the intermediate solvent regime the convergence is fairly good, whereas in the high solvent regime the convergence is very rapid. Clearly, the strength of coupling between the DNA and the heat bath affects in practice the convergence of important hydrodynamic properties.

G. Systematic versus frictional forces

To explore further the behavior at different viscosities, we show in Fig. 14 the ratio of the magnitude of the gradient to the magnitude of the friction (averaged over 10 000 iterations) as a function of γ [first to second term in the right-hand side of Eq. 1(a)]. There is a dramatic decrease of over eight orders of magnitude in this ratio as γ increases from 9.77×10^2 s^{-1} to 9.77×10^{12} s^{-1}. This explains and reinforces all analyses performed in this work. In the low γ regime, the DNA motion is entirely dominated by the systematic forces (the gradient of the potential energy is between two and eight orders of magnitude larger than the frictional force). At intermediate γ, frictional forces have a strong effect on the DNA motion but are not the dominant forces; the systematic force in this range is between two and ten times the frictional force. At high γ the frictional force is larger than the systematic forces and therefore dominates the motion of the DNA.

The effects of solvent-induced friction on the motion of the DNA can be seen qualitatively from Fig. 4. In the harmonic regime, where systematic forces dominate by several orders of magnitude (eight over the frictional forces), the DNA is globally harmonic (top row). In the intermediate γ regime (middle series) an interplay of random and inertial forces twist and bend the DNA fluidly through the solvent, though the random forces frequently reorient and reshape the polymer. When solvent damping is very strong (bottom sequence), the DNA macromolecule is entirely dominated by random forces and is virtually immobile.

IV. SUMMARY AND CONCLUSIONS

We have analyzed the effects of viscosity on the dynamics of supercoiled DNA. We wanted to explore the role of thermal damping in the natural cellular environ-

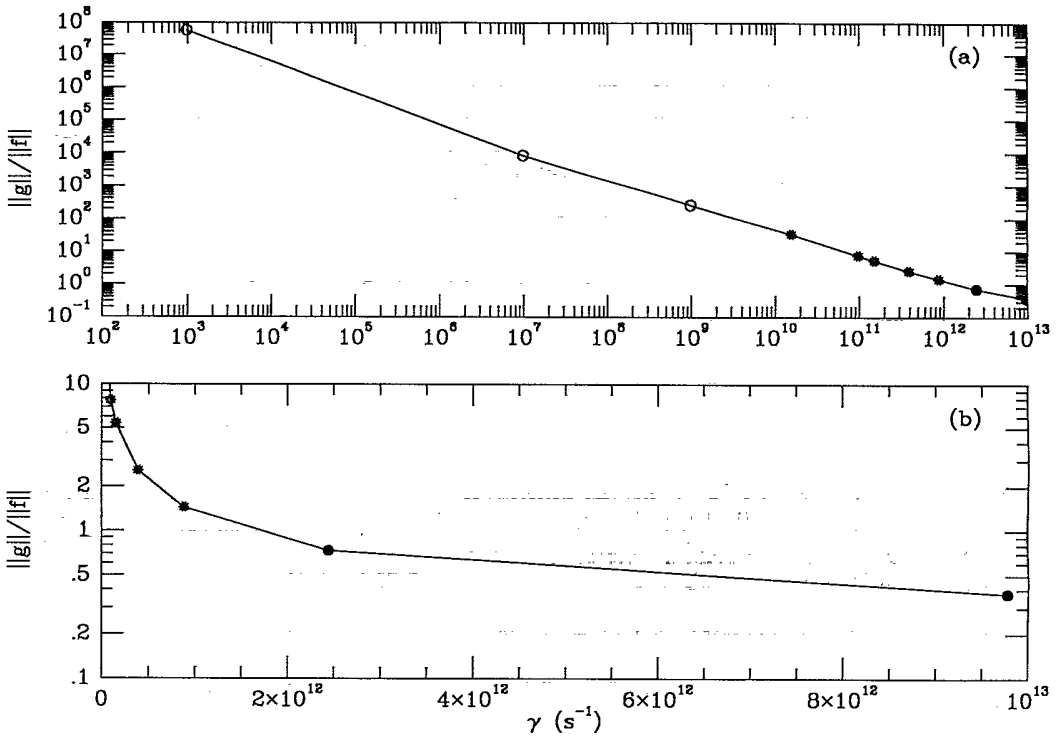

FIG. 14. Ratio of systematic to frictional forces in the Langevin formulation. The magnitude of the ratio of the systematic force to the frictional force (terms 1 and 2 on the left-hand side of [Eq. 1(a)], averaged over iterations 10 000 – 20 000, is plotted as a function of γ. Panel (a) is plotted on a log-log scale, and panel (b) is logarithmic only in the ordinate. Different symbols are used to distinguish points in the high (filled circles), medium (starred circles), and low (open circles) γ regimes.

ment and also to establish an optimal numerical tool. A systematic analysis of the influence of the solvent on both the statistical (sampling in finite time) and dynamical (kinetic) aspects of closed-circular DNA motion has been presented. The level of this analysis is qualitative and semiquantitative, compatible with our simplified macroscopic model of DNA, namely, that of a charged elastic rod. We summarize our main findings below.

(1) *Hydrodynamic effects on DNA motion.* Solvent viscosity plays a major role in determining DNA mobility. Solvent interactions do not indiscriminately overdamp all the internal global harmonic modes of DNA, but rather selectively activate or deactivate key internal modes. Thus as solvent density increases, a *qualitative* difference emerges in the motion of the supercoiled DNA. At low γ the DNA behaves in a globally harmonic fashion, and at high γ the inertial forces of the DNA are overdamped and transitions are infrequent. In the intermediate γ regime, however, the DNA is more mobile and flexible than at both extremes—significantly even more than the harmonic regime. The bending and twisting modes appear to have been activated at this critical viscosity, leading to enhanced configurational sampling in practice.

(2) *Accelerated sampling of free-energy minima.* Potential energy minimization from the circle and the interwound structure lead to a single, tightly interwound structure with Wr = 2.05 at the particular set of parameters used here. The accelerated sampling seen in the intermediate γ regime, however, reveals more favored configurations that are significantly less tightly wound than the enthalpic minimum. They cluster near configurations with Wr = 1.4. It is thus possible that thermal fluctuations lead to configurational states that are energetically competitive with the enthalpic minimum. At high γ, we still note transitions to this free-energy minimum, but they are infrequent over the same simulation length due to the deactivation of the global modes, apparently necessary for concerted motions. This evidence of a free-energy minimum, distinct from the enthalpic minimum, further underscores the importance of considering thermal effects on DNA structure and mobility in solution.

(3) *DNA sampling in solution as a barrier crossing event.* The configurational sampling of the DNA as a function of γ bears a strong resemblance to the transition-rate dependence on γ of a particle in a bistable potential—the archetypal barrier crossing problem. This interesting similarity suggests that the sampling of the two free-energy minima by the DNA could be described as a condensed-phase barrier crossing event. Here, the solvent might serve to activate the reaction path by turning on or off specific internal modes. The mechanism for mode activation is still not well understood for the simple case (particle in a bistable potential), but it is fascinating that a problem of much greater complexity, such as

DNA dynamics, shares similar characteristics. By analogy to the particle in a bistable potential, we suggest that a global twisting mode describes the pathway for transition between the two minima.

The above results show that solvent in the DNA environment exerts a profound *qualitative* and *quantitative* influence on the dynamical behavior of supercoiled DNA. This influence is more than just a systematic trend of overdamping as a function of γ, but rather one which isolates distinct physical regimes of DNA behavior. Computationally, a moderate viscosity is favorable, because it enhances configurational sampling significantly and thus leads to more rapid convergence of equilibrium distributions. On the basis of the physical and computational considerations discussed throughout this work, we conclude that an appropriate choice of γ for our model lies in the intermediate γ regime (10^{11} s^{-1} $< \gamma <$ 10^{12} s^{-1}). This viscosity regime incorporates appropriate solvent damping and, therefore, the thermal fluctuations expected from long floppy DNA systems. In addition, configurational sampling is increased significantly due to an optimal balance between internal and frictional forces. Further explorations of the biological implications of such solvent and solute dynamic interactions in topologically constrained DNA systems will be reported separately [12].

ACKNOWLEDGMENTS

We thank Constantine Kreatsoulas and Edward Friedman for their help with computer graphics and Wilma K. Olson, Susan Tucker, and Alexander Vologodskii for valuable comments. Our research was generously supported by the National Science Foundation (Grant Nos. CHE-9002146, ASC-9157582, and ASC-9318159, the latter cofunded by ARPA), the National Institutes of Health (Grant Nos. RR08102 and CI-0474), and the Whitaker and Alfred P. Sloan Foundations. T.S. is an investigator of the Howard Hughes Medical Institute.

[1] J. C. Wang, J. Mol. Biol. **43**, 25 (1969).
[2] C. F. Anderson and W. Bauer, Biochemistry **17**, 594 (1978).
[3] S. Y. Shaw and J. C. Wang, Science **260**, 533 (1993).
[4] V. V. Rybenkov, N. R. Cozzarelli, and A. V. Vologodskii, Proc. Natl. Acad. Sci. USA **90**, 5307 (1993).
[5] J. Langowski and U. Geisen, Biophys. Chem. **34**, 9 (1989).
[6] G. W. Brady, M. Satkowski, D. Foos, and C. J. Benham, J. Mol. Biol. **195**, 185 (1987).
[7] A. V. Vologodskii and N. R. Cozzarelli, Curr. Opin. Struct. Biol. **4**, 372 (1994); T. Schlick, Curr. Opin. Struct. Biol. **5**, 245 (1995).
[8] T. Schlick and W. K. Olson, J. Mol. Biol. **223**, 1089 (1992).
[9] T. Schlick, B. Li, and W. K. Olson, Biophys. J. **67**, 2146 (1994).
[10] R. W. Pastor, in *The Molecular Dynamics of Liquid Crystals*, edited by G. R. Luckhurst and C. A. Veracini (Kluwer Academic Press, Dordrecht, 1994), pp. 85–138.
[11] S. Chandrashekar, Rev. Mod. Phys. **15**, 1 (1943).
[12] G. Ramachandran and T. Schlick (unpublished).
[13] D. L. Beveridge and G. Ravishanker, Curr. Opin. Struct. Biol. **4**, 246 (1994).
[14] B. Jayaram and D. L. Beveridge, J. Phys. Chem. **95**, 2506 (1991).
[15] R. J. Loncharich, B. R. Brooks, and R. W. Pastor, Biopolymers **32**, 523 (1992).
[16] R. Risken, *The Fokker-Planck Equation* (Springer-Verlag, Berlin, 1989).
[17] H. A. Kramers, Physica **7**, 284 (1940).
[18] T. Schlick, W. K. Olson, T. Westcott, and J. P. Greenberg, Biopolymers **34**, 565 (1994).
[19] V. I. Mel'nikov and S. V. Meshkov, J. Phys. Chem. **85**, 1018 (1986).
[20] A. Nyberg and T. Schlick, J. Chem. Phys. **95**, 4986 (1991).
[21] H. Eyring, J. Phys. Chem. **3**, 107 (1935).
[22] P. J. Kraulis, J. Appl. Crystallogr. **24**, 946 (1991).
[23] C. S. Peskin and T. Schlick, Comm. Pure Appl. Math. **42**, 1001 (1989).
[24] T. Schlick *et al.*, in *Theoretical Biochemistry and Molecular Biophysics*, edited by D. L. Beveridge and R. Lavery (Adenine Press, Schenectady, New York, 1991), Vol. 1, pp. 39–58.
[25] T. Schlick, B. Li, and M.-H. Hao, in *Structural Biology: State of the Art 1993, Proceedings of the Eighth Conversations, Volume I*, edited by R. Sarma and M. Sarma (Adenine Press, Schenectady, New York, 1994), pp. 157–174.
[26] G. Zhang and T. Schlick, J. Comput. Chem. **14**, 1212 (1993).
[27] J. H. White, in *Mathematical Methods for DNA Sequences*, edited by M. S. Waterman (CRC Press, Boca Raton, FL, 1989), Chap. 9.
[28] D. Sprous II, R. K.-Z. Tan, and S. C. Harvey (unpublished).
[29] A. Sokal, *Monte Carlo Methods in Statistical Mechanics: Foundations and New Algorithms* (Cours de Troisième Cycle de la Physique en Suisse Romande, Lausanne, 1989).
[30] R. S. Dumont, J. Chem. Phys. **96**, 2203 (1992).
[31] M. P. Allen and D. J. Tildesley, *Computer Simulation of Liquids* (Clarendon Press, Oxford, England, 1987).
[32] P. E. Smith and W. F. van Gunsteren, J. Mol. Biol. **236**, 629 (1994).